

Self-similarity and scaling behavior of IR emission from radiatively heated dust: I. Theory

Željko Ivezić and Moshe Elitzur

Department of Physics and Astronomy, University of Kentucky, Lexington, KY 40506-0055, USA

e-mail: ivezic@pa.uky.edu, moshe@pa.uky.edu

Accepted December 16, 1996. Received September 30, 1996; in original form July 17, 1996

ABSTRACT

Dust infrared emission possesses scaling properties that yield powerful results with far reaching observational consequences. Scaling was first noticed by Rowan-Robinson for spherical shells and is shown here to be a general property of dust emission in arbitrary geometries. Overall luminosity is never an input parameter of the radiative transfer problem, spectral shape is the only relevant property of the heating radiation when the inner boundary of the dusty region is controlled by dust sublimation. Similarly, the absolute scales of densities and distances are irrelevant; the geometry enters only through angles, relative thicknesses and aspect ratios, and the actual magnitudes of densities and distances enter only through one independent parameter, the overall optical depth. That is, as long as the overall optical depth stays the same, the system dimensions can be scaled up or down by an arbitrary factor without any effect on the radiative transfer problem. Dust properties enter only through dimensionless, normalized distributions that describe the spatial variation of density and the wavelength dependence of scattering and absorption efficiencies.

Scaling enables a systematic approach to modeling and classification of IR spectra. We develop a new, fully scale-free method for solving radiative transfer, present exact numerical results, and derive approximate analytical solutions for spherical geometry, covering the entire range of parameter space relevant to observations. For a given type of grains, the spectral energy distribution (SED) is primarily controlled by the profile of the spatial dust distribution and the optical depth — each density profile produces a family of solutions, with position within the family determined by optical depth. From the model SEDs presented here, the density distribution and optical depth can be observationally determined for various sources.

Scaling implies tight correlations among the SEDs of various members of the same class of sources such as young stellar objects, late-type stars, etc. In particular, all members of the same class occupy common, well defined regions in color-color diagrams. The observational data corroborate the existence of these correlations.

Key words: infrared – dust – radiative transfer – stars: late-type – young stellar objects

1 INTRODUCTION

For many astronomical objects, the radiation we receive has undergone significant processing by surrounding dust, and its detailed interpretation requires considerable theoretical effort. Input to the necessary radiative transfer calculations includes properties of the original radiation, optical characteristics of individual dust grains, and the dust density distribution. Specifying all the relevant properties traditionally involved a rather large number of input parameters, creating two major practical problems. First, the volume of pa-

rameter space that must be searched to fit a given set of observations can become prohibitively large. Second, and more serious, even when a successful fit is accomplished, its uniqueness is questionable and the model parameters cannot be trusted as a reliable indication of the source actual properties.

In fact, much of this input is redundant because the radiative transfer problem possesses general scaling properties that drastically reduce the number of independent input parameters. Rowan-Robinson (1980, RR hereafter) was the first to utilize scaling in his extensive study of IR emission

from spherical dust shells. In his formulation of the radiative transfer problem, the overall luminosity, as well as other quantities, never enters. The full power of this scaling was exploited in our previous work on late-type stars (Ivezić & Elitzur 1995, IE95 hereafter). There we show that, given the dust optical properties, for each circumstellar shell both the dynamics and IR emission are successfully described by a single parameter – the overall optical depth. This explains the many correlations displayed by the data for late-type stars. Here we derive the general form of these results, extending the scaling analysis to arbitrary geometries and density distributions. Formal discussion of the general scaling properties of the radiative transfer equation is presented in Section 2, and applied in Section 3 to radiatively heated dust in arbitrary geometries. In Section 4, more detailed, concrete results are derived for spherically symmetric systems, leading to a new, exact method for solution of the radiative transfer problem that can be readily extended to arbitrary geometries. Thanks to scaling, the effects of the independent input properties on emerging radiation can be searched systematically. In Section 5 we present such an exhaustive search for spherical systems and the entire relevant range of input properties. We explore the effects of various density distributions, grain size and chemical composition, sublimation temperature, and spectral shape of the external radiation. Section 6 contains a summary of our results and a discussion of observational implications. A subsequent paper will present detailed analysis of the IRAS data base, which displays strong evidence for the scaling properties derived here.

2 GENERAL SCALING PROPERTIES

The equation of radiative transfer in steady-state is

$$\frac{dI_\lambda}{d\ell} = \kappa_\lambda(S_\lambda - I_\lambda). \quad (1)$$

Here κ_λ is the overall extinction coefficient at wavelength λ including both absorption and scattering, $\kappa_\lambda = \kappa_{a\lambda} + \kappa_{s\lambda}$, and the corresponding optical depth element along the path is $d\tau_\lambda = \kappa_\lambda d\ell$. We will also make use of the albedo $\varpi_\lambda = \kappa_{s\lambda}/\kappa_\lambda$. In addition to boundary conditions, solution of this equation for the intensity I_λ requires two input functions at every point \mathbf{r} – the source function $S_\lambda(\mathbf{r})$ and the absorption coefficient $\kappa_\lambda(\mathbf{r})$. The equation involves quantities with dimensions of either intensity or length. The intensity I_λ and source function S_λ belong to the first type, the path-length ℓ and absorption coefficient κ_λ , which has dimensions of inverse length, to the second. Therefore the formulation of any radiative transfer problem can involve only two dimensional scales, one for intensities the other for lengths. All other relevant scales must be dimensionless, involving ratios with the two dimensional scales.

2.1 Length Scales

Consider first the length-type quantities. Because all distances can be replaced by equivalent dimensionless τ_λ , the radiative transfer problem is independent of linear size scales. The only geometrical properties that can enter the

problem involve angular sizes and the spatial variation of optical depth. To further explore this scaling, introduce some arbitrary length scale r_1 . Any position $\mathbf{r} = (r, \theta, \phi)$ can be specified instead by the dimensionless vector $\mathbf{y} = (y, \theta, \phi)$, where

$$y = r/r_1 \quad (2)$$

is dimensionless distance from the (arbitrary) origin. Denote a radiative transfer path by \mathcal{P} and positions along this path by $(y; \mathcal{P})$, where yr_1 is distance from the path's closest approach to the origin. Then the path-length element is $d\ell = r_1 dy$ and the radiative transfer equation (1) becomes

$$\frac{dI_\lambda(y; \mathcal{P})}{dy} = \tau_\lambda^T(\mathcal{P})\eta(y; \mathcal{P})[S_\lambda(y; \mathcal{P}) - I_\lambda(y; \mathcal{P})]. \quad (3)$$

Here $\tau_\lambda^T(\mathcal{P})$ is the total optical depth along the path at wavelength λ and

$$\eta(y; \mathcal{P}) = \frac{1}{\tau_\lambda^T(\mathcal{P})} \frac{d\tau_\lambda(y; \mathcal{P})}{dy} = \frac{\kappa_\lambda(y; \mathcal{P})}{\int \kappa_\lambda(y; \mathcal{P}) dy} \quad (4)$$

is a dimensionless function that describes the spatial variation of opacity. In general $\eta(y; \mathcal{P})$ depends also on wavelength. This dependence disappears when the properties of individual absorbers do not vary with position, in which case $\eta(y) = n_a(y)/\int n_a(y) dy$, the normalized dimensionless density distribution of absorbers. If in addition the absorber abundance does not vary, i.e., n_a/n is constant, η becomes simply the normalized dimensionless density distribution $n(y)/\int n(y) dy$.

In its new form, the radiative transfer equation (3) no longer contains any quantities with dimensions of length; physical dimensions enter only as ratios, i.e., angles and aspect ratios. Furthermore, the length scale r_1 has disappeared altogether, thus it is not required for a complete solution. This quantity enters into the problem only through the product $r_1\kappa_\lambda = \tau_\lambda^T\eta$. Therefore, any scale associated with it is contained in the overall optical depth τ_λ^T because the function η sets its own scale from the normalization

$$\int \eta(y; \mathcal{P}) dy = 1 \quad (5)$$

for any path \mathcal{P} . This shows that *radiative transfer is scale invariant*. The physical dimensions of any system can be scaled up and down arbitrarily without any effect on its radiative properties as long as optical depths and relative matter distribution remain the same. Two systems with entirely different dimensions and absorption coefficients but the same overall optical depths will produce the same radiative intensities if they have self-similar distributions of opacities and source functions. Since the length scale r_1 does not enter into the radiative transfer problem, a corollary is that it can never be determined from the solution. The only way to determine actual length scales is through some independent determination of the size of the system or the distance to it.

The scale-invariance of radiative transfer reflects the fact that, in principle, the problem could be formulated using optical depth as the independent variable, differentiating with respect to $d\tau_\lambda(y; \mathcal{P}) = \tau_\lambda^T(\mathcal{P})\eta(y; \mathcal{P}) dy$. In that case, location in space (the argument of I_λ and S_λ) is specified by its optical depth along the chosen path, $\tau_\lambda(y; \mathcal{P}) = \tau_\lambda^T(\mathcal{P}) \int^y \eta(u; \mathcal{P}) du$. This scale-invariant formu-

lation is completely general and applies to all geometries, including irregular shapes, clumpy media, etc. In this general form, the path-dependent function $\eta(y; \mathcal{P})$ describes the geometrical morphology, in essence defining the transformation from real space to τ -space, which might be quite involved. In cases of geometrical symmetry, radiative transfer is more conveniently formulated with τ defined along the axis of symmetry. Then $\eta(y)$ is defined in an analogous manner, for example along the radial direction in the case of spherical symmetry (cf Section 4).

3 HEATED DUST

The discussion so far was general and applies to all radiative problems without restrictions. In practice, the scale invariance is mostly useful when the absorption coefficient is independent of intensity, and from here on we concentrate on such systems. Thus the following discussion excludes line emission and photoionization (where the absorption coefficient may depend on intensity through its effect on level populations), but is fully applicable to continuum radiation – especially by dust, the main thrust of this paper. With this restriction, in the absence of a source function radiative transfer would be described by a homogeneous equation. That is, if I_λ is a solution when the source term is removed then so is aI_λ for any arbitrary constant a . This scale invariance is broken by the source term, which makes the radiative transfer equation inhomogeneous. In the case of a dusty medium, the source function is

$$S_\lambda = (1 - \varpi_\lambda)B_\lambda(T) + \varpi_\lambda \int I_\lambda(\Omega')g(\Omega', \Omega) \frac{d\Omega'}{4\pi}, \quad (6)$$

where B_λ is the Planck function and $g(\Omega', \Omega)$ is the angular phase function for coherent scattering from direction Ω' to Ω (e.g. Mihalas 1978). Because of scattering, in general S_λ contains a dependence on directions. We assumed for simplicity single-type dust grains, characterized by a single temperature T . The general grain mixture case is similar in all fundamental aspects and is discussed separately in appendix A.

Since the scattering term is linear in I_λ , it preserves the scale invariance of intensity. The only term to break this invariance and set a scale for the intensity is the emission term, $B_\lambda(T)$. It does that by introducing the dust temperature, determined from radiative equilibrium

$$\int d\Omega \int \kappa_\lambda S_\lambda d\lambda = 4\pi \int \kappa_\lambda J_\lambda d\lambda, \quad (7)$$

where $J_\lambda = \int I_\lambda d\Omega/4\pi$ is the angle-averaged intensity. Both sides of this relation vary linearly with the extinction coefficient, therefore the actual magnitude of this quantity is irrelevant – only its wavelength variation matters. Indeed, Leung (1976) noticed from his numerical calculations that T was “rather insensitive” to the absolute values of extinction coefficient; our discussion shows that this insensitivity is in fact an exact symmetry property of the problem. To emphasize this point we write this relation in terms of

$$q_\lambda = \frac{\kappa_\lambda}{\kappa_{\lambda_0}}, \quad (8)$$

the extinction coefficient normalized to unity at some fiducial, arbitrary wavelength λ_0 .^{*} With the dust source function from equation 6, the radiative equilibrium condition becomes

$$\int q_{a\lambda} B_\lambda(T) d\lambda = \int q_{a\lambda} J_\lambda d\lambda, \quad (9)$$

where $q_{a\lambda} = q_\lambda(1 - \varpi_\lambda)/(1 - \varpi_{\lambda_0})$ is the absorption efficiency normalized to the fiducial wavelength λ_0 . Because the scattering term preserves scale invariance, it does not enter into this scale-setting equation (which therefore becomes meaningless in the case of pure scattering, $\varpi_\lambda = 1$).

The actual energy input into the dust is external radiation from a nearby source, such as a star, galactic nucleus, etc., of radius r_e and intensity $I_{e\lambda}$. When this source is non-spherical (for example disk or torus), the angular profile of its geometrical shape, too, must be specified. The dust distribution has some prescribed arbitrary geometrical shape and we denote the distance of its closest point to the source of radiation r_1 . From the previous section, the radiative transfer problem can not depend separately on r_e or r_1 , only on their ratio

$$\theta_{e1} = \frac{r_e}{r_1}. \quad (10)$$

Therefore, the only geometrical property of the radiation source relevant to the problem is its angular size at the location of the dust (and its angular shape profile when it is non-spherical). The radiative input to the dust can be characterized by the external flux at r_1 ,

$$F_{e\lambda}(r_1) = \int \mu I_{e\lambda} d\Omega \approx \pi \theta_{e1}^2 I_{e\lambda}. \quad (11)$$

This spectral distribution can be specified instead by its scale, the bolometric flux at r_1

$$F_{e1} = \int F_{e\lambda}(r_1) d\lambda = \frac{L_e}{4\pi r_1^2}, \quad (12)$$

where L_e is the luminosity, and spectral shape

$$f_{e\lambda} = \frac{F_{e\lambda}}{F_e}, \quad (13)$$

an r -independent normalized distribution ($\int f_{e\lambda} d\lambda = 1$). Then $F_{e\lambda}(r_1) = f_{e\lambda} F_{e1}$. Consider now the series of models in which all properties are held fixed except the input bolometric flux F_{e1} . Each value of F_{e1} uniquely determines a corresponding value of T_1 , the dust temperature at r_1 . This in turn defines another flux σT_1^4 , setting the intrinsic scale of dust emission. But the radiative transfer problem can involve only one radiative scale, therefore the ratio of these two fluxes must be a characteristic dimensionless function of the model. That is, the ratio

$$\Psi = \frac{4\sigma T_1^4}{F_{e1}} \quad (14)$$

is uniquely determined by the dimensionless properties of the model such as optical depths, angular shapes and dimensionless density profile (the factor 4 is introduced for

^{*} Although the absolute value of κ_λ does not enter independently into the radiative transfer problem, it is needed to relate the optical depth to the total dust mass.

convenience). It may also depend on ratios of opacity spectral averages involving the profile $f_{e\lambda}$ of the input radiation and

$$b_\lambda(T_1) = \frac{\pi}{\sigma T_1^4} B_\lambda(T_1), \quad (15)$$

the normalized ($\int b_\lambda d\lambda = 1$) spectral shape of the Planck distribution at temperature T_1 . However, it can not depend on any dimensional quantity such as luminosity, linear size or density. In Section 5 we present results for Ψ in spherical symmetry (figure 1) and derive an analytic approximation for its τ -dependence (equation 33).

This discussion shows that the luminosity never enters into the formulation of the radiative transfer problem, only the input flux matters. And rather than specifying the flux scale, the dust temperature can be specified instead so that flux becomes a derived quantity. *A dusty region with prescribed properties can transport only a single, well defined radiative flux for a given dust temperature on its heated boundary.* It is determined from the full solution through the scaling function Ψ , which can be viewed as an eigenvalue of the model. The fact that the radiative transfer problem can be fully specified in terms of temperatures rather than radiative flux was first utilized in RR for spherical shells. Equation 14 is the general form of this property for all geometries.

Dust sublimation occurs at some temperature T_{sub} , determined by the grain properties. As long as the input flux F_{e1} is sufficiently low that $T_1 < T_{\text{sub}}$, the dust temperature at the inner boundary varies according to eq. 14 ($T_1 \propto F_{e1}^{1/4}$) and different luminosities produce dust emission that differs both in overall luminosity and spectral shape. This is generally the situation in planetary nebulae. However, once F_{e1} increases to the point that $T_1 = T_{\text{sub}}$, the dust temperature cannot rise any more. Instead, further increases in luminosity move out the inner boundary of the dust so that F_{e1} remains fixed at the value that produces $T_1 = T_{\text{sub}}$. Thus the temperature profile and emission of the dust are set by its internal properties in this regime. Stated differently – since F_{e1} uniquely determines T_1 , the converse is also true and T_1 uniquely determines a corresponding F_{e1} . Models in which the dust is as close to the radiation source as possible have the same T_1 and therefore adjust their inner boundary to accommodate the external luminosity so that they also have the same F_{e1} . Since the bolometric flux is now self-regulated by dust sublimation, *when the dust is as close to the radiation source as possible, the only relevant property of the input radiation is its spectral shape $f_{e\lambda}$.*

In this discussion we assumed single-component dust and heating by a single external radiative source. Multi-component dust mixtures are discussed in Appendix A which shows that, although the technical complications increase, all the essential scaling properties are preserved. The same applies to heating by more than one source. Because radiative transfer can involve only one intensity scale, the addition of an external source can only introduce the ratio of corresponding fluxes $F_{e\lambda}$ at every point.

4 SPHERICAL SYMMETRY

To further explore concrete consequences of general scaling we must specify the geometry. Here we take the case of

spherical symmetry. The essence of most results is preserved in other geometries.

In the case of spherical symmetry, y can be taken as dimensionless distance from the center of symmetry, and τ_λ^T and $\eta(y)$ defined along the radial path. The radiation source is surrounded by a spherical dust shell with inner radius r_1 corresponding to dust sublimation, which we choose as the scaling length in equation 2. With this choice, dust sublimation always occurs at $y = 1$ and the dust temperature scale is set by $T(y=1) \equiv T_1 = T_{\text{sub}}$. The dust optical properties are fully specified by the wavelength variation of the absorption efficiency $q_{a\lambda}$ and the albedo ϖ_λ . Its spatial distribution is described by

$$\eta(y) = \frac{\kappa_\lambda(y)}{\int_1^\infty \kappa_\lambda(y) dy}, \quad (16)$$

the dimensionless variation of extinction coefficients in the radial direction. Note again that $\eta(y)$ does not introduce a new scale since it is normalized via $\int_1^\infty \eta(y) dy = 1$. When the dust properties do not vary with distance beyond the sublimation point, η describes the radial law of density variation, e.g., y^{-2} , $\exp(-y)$, etc. There is no need to specify the actual density itself. The extinction scale is set by τ_0 , the total optical depth along radial rays at the fiducial wavelength λ_0 . At all other wavelengths, $\tau_\lambda^T = \tau_0 q_\lambda$. At any point y , the optical depth from the closest approach to the center along a path that makes an angle θ with the radius vector is

$$\tau_\lambda(y, \theta) = \tau_\lambda^T \int_0^{y \cos \theta} \eta \left(\sqrt{u^2 + y^2 \sin^2 \theta} \right) du. \quad (17)$$

Rowan-Robinson was the first to incorporate geometrical scaling for spherical shells into a formalism that specifies only scaled radii, τ_λ^T and η .

From the formal solution of the radiative transfer equation, the intensity at radius y of a ray inclined at angle θ to the radial direction is

$$I_\lambda(y, \theta) = I_{e\lambda} e^{-\tau_\lambda(y)} \Theta \left(\frac{\theta_{e1}}{y} - \theta \right) + I_{d\lambda}(y, \theta). \quad (18)$$

Here Θ is the step function (unity for positive arguments, zero otherwise) and

$$I_{d\lambda}(y, \theta) = \int S_\lambda(y', \theta) e^{\tau_\lambda(y', \theta) - \tau_\lambda(y, \theta)} d\tau_\lambda(y', \theta) \quad (19)$$

is the intensity of the diffuse radiation. By angular integration, the angle-averaged intensity is similarly

$$J_\lambda(y) = \frac{F_{e1}}{4\pi y^2} f_{e\lambda} e^{-\tau_\lambda(y)} + J_{d\lambda}(y), \quad (20)$$

where $J_{d\lambda}$ denotes the diffuse component. We now show that $J_{d\lambda}$, which is comprised of dust emission and scattering, can be expressed explicitly in terms of J_λ . For the emission term this result is straightforward since this term is controlled by the dust temperature T , determined from

$$q_{aP}(T) T^4 = q_{aP}(T_1) T_1^4 \frac{\int q_{a\lambda} J_\lambda(y) d\lambda}{\int q_{a\lambda} J_\lambda(1) d\lambda} \quad (21)$$

(cf equation 9). Here we introduced the Planck mean of the absorption efficiency

$$q_{aP}(T) = \int q_{a\lambda} b_\lambda(T) d\lambda. \quad (22)$$

For the scattering component, consider first the case of isotropic scattering, $g(\Omega', \Omega) = 1$. Then the scattering term in the source function is simply $\varpi_\lambda J_\lambda$ (eq. 6), and the entire diffuse component $J_{d\lambda}$ becomes an explicit function of J_λ . Similarly, for the external radiation, radiative equilibrium at $y = 1$ (where $T = T_1$) determines the input bolometric flux F_{e1} , or equivalently Ψ (see eq. 14), as

$$\Psi = \frac{q_{ae}}{q_{aP}(T_1)} \frac{1}{1 - \epsilon} \quad (23)$$

where

$$q_{ae} = \int q_{a\lambda} f_{e\lambda} d\lambda, \quad \epsilon = \frac{\int q_{a\lambda} J_{d\lambda}(1) d\lambda}{\int q_{a\lambda} B_\lambda(T_1) d\lambda}. \quad (24)$$

Since $J_{d\lambda}$ is an explicit function of J_λ , the same holds for Ψ . Therefore, the entire right-hand-side of equation 20 is expressed explicitly in terms of J_λ , so this is a self-consistency equation for the unknown J_λ whose only inputs are dust properties and the spectral shape of incoming radiation. As an inhomogeneous integral equation, it has a unique physical solution. This completes the formulation of the radiative transfer problem in accordance with the general scaling discussion of the previous section. The only property of the external radiation that needs to be specified as input is its spectral shape $f_{e\lambda}$.

Anisotropic scattering can be handled similarly. In that case we write $I_\lambda(\theta) = \Phi(\theta)J_\lambda$, where Φ is the intensity angular distribution, normalized as $\int \Phi d\Omega = 4\pi$. Equation 20 for J_λ remains the same, only the scattering contribution to $J_{d\lambda}$ includes now an integral over Φ . The only technical complication is the need to additionally solve the coupled equation (18) for the angular distribution Φ . The rest of the formulation is the same as for isotropic scattering. In complete analogy, arbitrary geometries can be handled through equally straightforward extensions.

Solution of equation 20 for J_λ determines the radial variation of the source function in the shell. Once this function is known, the flux and surface brightness, the quantities relevant for observations, are readily calculated. In particular, the overall flux is obtained from the first-moment angular integration of equation 18 which yields

$$F_\lambda(y) = \frac{F_{e1}}{y^2} f_{e\lambda} e^{-\tau_\lambda(y)} + F_{d\lambda}(y), \quad (25)$$

similar to the expression for J_λ . As with the external radiation, it is convenient to remove the overall scale, contained in the bolometric flux $F = \int F_\lambda d\lambda$. The spectral shape of the overall flux is denoted f_λ , so that

$$F_\lambda(y) = f_\lambda(y)F(y), \quad F(y) = \frac{F_1}{y^2}. \quad (26)$$

Here F_1 is the bolometric flux at $y = 1$, including both external and dust contributions, and the second equality expresses flux conservation.

The luminosity L_e has never entered, and is irrelevant. It is important to note, however, that the bolometric flux F_1 is fully determined even though the overall luminosity is not. This flux combines the dimensional scales L_e and r_1 which otherwise do not enter individually, thus dropping out of the problem. The corresponding relation, obtained by combining equations 12 and 14, can be written as

$$r_1^2 = \frac{L_e}{16\pi\sigma T_1^4} \Psi = \frac{\Psi}{4} r_c^2 \left(\frac{T_{\text{eff}}}{T_1} \right)^4, \quad (27)$$

where the last equality is written in terms of the source's effective temperature T_{eff} . This is the exact expression of a result noted in various forms by RR, Laor & Draine (1993) and Ivezić & Elitzur (1996a; IE96 hereafter). Therefore, when the overall luminosity is known, it can be used to determine the radius of the dust sublimation zone.

The only properties of the central source that affect the observed radiation are its spectral shape $f_{e\lambda}$ and angular size θ_{e1} . The latter enters explicitly only in the expression for the intensity, eq. 18, thus it can be determined directly only in high-resolution observations that delineate the external contribution as a bright spot. In most cases, though, the central source is unresolved and the quantity relevant for observations is the flux. The angular integration that transforms intensity to flux removes the explicit dependence on θ_{e1} , as is evident from eq. 25, but the flux may still depend on θ_{e1} because of occultation of the diffuse radiation by the central source. Without occultation, the diffuse flux would vanish at r_1 because the intensities of the two streams along any ray are then the same (Milne, 1921). Thus the significance of occultation can be gauged from the ratio $F_d(r_1)/F_{e1}$ of the diffuse and external contributions to the bolometric flux at r_1 . Only rays occulted by the central source contribute to $F_{d\lambda}(r_1)$, and $B_\lambda(T_1)$ is an upper limit to their intensity. Therefore, $F_{d\lambda}(r_1) < \pi\theta_{e1}^2 B_\lambda(T_1)$ at all wavelengths and

$$\frac{F_d(r_1)}{F_{e1}} < \left(\frac{T_1}{T_{\text{eff}}} \right)^4. \quad (28)$$

Occultation can be ignored whenever $T_1 \ll T_{\text{eff}}$. Comparison with eq. 27 shows that this condition is equivalent to $\theta_{e1}^2 \Psi \ll 1$. When this condition is obeyed,

$$F_1 = F_{e1}, \quad f_\lambda(y) = f_{e\lambda} e^{-\tau_\lambda(y)} + y^2 F_{d\lambda}(y)/F_1, \quad (29)$$

and the problem is independent of θ_{e1} . Therefore, as long as $T_{\text{eff}} \gg T_{\text{sub}} = T_1$, the only relevant property of the central source is its spectral shape $f_{e\lambda}$; T_{eff} is irrelevant, and in the remainder of the discussion we assume that this condition is fulfilled.[†] When T_{eff} decreases and approaches T_{sub} , a dependence on angular size θ_{e1} enters, but T_{eff} itself remains irrelevant as long as $T_1 = T_{\text{sub}}$ is maintained. Finally, scaling breaks down when T_{eff} is so small that $T_1 < T_{\text{sub}}$. In this case, T_{eff} must be specified, too, since it determines T_1 . This breakdown of scaling occurs also when the central cavity is dust-free because of factors other than dust sublimation, such as dynamics for example, and $T_1 < T_{\text{sub}}$.

5 IMPLICATIONS

When the dust is optically thin at all wavelengths, the solution is straightforward. Inserting $\tau_\lambda \sim 0$ and neglecting the diffuse emission, equation 20 gives $J_\lambda(y) = J_\lambda(1)/y^2$ and so

$$\frac{q_{aP}(T)}{q_{aP}(T_1)} \left(\frac{T}{T_1} \right)^4 = \frac{1}{y^2}, \quad \Psi = \frac{q_{ae}}{q_{aP}(T_1)}. \quad (30)$$

Most of the contribution to the Planck mean comes from the distribution peak around

[†] For a more detailed discussion of backwarming effects see Rowan-Robinson (1982).

$$\lambda_p(T) = 4 \mu\text{m} \frac{1000 \text{ K}}{T}, \quad (31)$$

so $q_{\text{aP}}(T) \simeq q_{\text{a}\lambda_p(T)}$. If the corresponding wavelength is in the regime where the absorption efficiency drops as a power law, $q_{\text{a}\lambda} \propto \lambda^{-\beta}$, we recover the familiar result for the dust temperature $T = T_1 y^{-2/(4+\beta)}$. Also, when the spectral shape of the external radiation is that of a black-body with temperature T_e , the optically thin limit of Ψ becomes

$$\Psi(\tau = 0) \simeq \frac{q_{\text{a}\lambda_p(T_e)}}{q_{\text{a}\lambda_p(T_1)}}, \quad (32)$$

that is, it is determined by the drop in absorption efficiency between the wavelengths corresponding to the temperatures of the external source and dust sublimation.

When the dust is optically thick the problem must be solved numerically, and we have developed a computer code (DUSTY; Ivezić, Nenkova & Elitzur 1997) to solve the spherical problem. A description of the numerical procedure is provided in Appendix C. Our program solves equation 20 for $J_\lambda(y)$, with the dust temperature determined from equation 21 and the flux scale $F_1 = 4\sigma T_1^4 \Psi$ from equation 23. Input includes the optical properties $q_{\text{a}\lambda}$ and ϖ_λ , the dust sublimation temperature T_{sub} , its density distribution η and the external spectral shape $f_{e\lambda}$. A given set of these quantities defines a family of solutions, distinguished from each other by overall optical depth. Matching a model to observations provides the optical depth of the source if there are independent estimates for the other properties. Note that the only effects on the spectral energy distribution that can be meaningfully discerned in observations involve changes of spectral features or of slope.

We present now the results of exact calculations, first for what we will use as a “standard” model with $\eta = y^{-2}$, single-component dust grains with size $a = 0.05 \mu\text{m}$ and sublimation temperature $T_{\text{sub}} = 700 \text{ K}$, and external radiation with the spectral shape of a black body with $T_e = 2500 \text{ K}$. We then explore the effects of different input quantities on the emergent flux and discuss the behavior of the solutions with the aid of analytic approximations developed in Appendix B. In all cases we vary τ_V , the overall optical depth at $0.55 \mu\text{m}$, all the way to 1000 and present solutions for both amorphous carbon and silicate grains. Optical properties for the former are taken from Hanner (1988), for the latter from Ossenkopf, Henning & Mathis (1992). The scattering is assumed isotropic. Similar explorations of parameter space were performed by Leung and by Rowan-Robinson. In addition to employing updated optical properties, the coverage presented here is more extensive and the systematics of the presentation more closely reflect scaling.

Figure 1 displays the variation of Ψ with τ_V . For each chemical composition, the optically thin value is a measure of the drop in absorption between $\lambda_p(T_e) \simeq 2 \mu\text{m}$ and $\lambda_p(T_{\text{sub}}) \simeq 6 \mu\text{m}$ (equation 32). The thin lines are the analytic results of equation B7, seen to provide excellent approximations to the exact calculations. These analytic expressions are not too transparent as they involve spectral integrations of the detailed extinction efficiencies. Therefore, we discuss the results instead in terms of the gray-opacity approximation, equation B9, which maintains most of the main features. In particular, it explains the rise of Ψ with

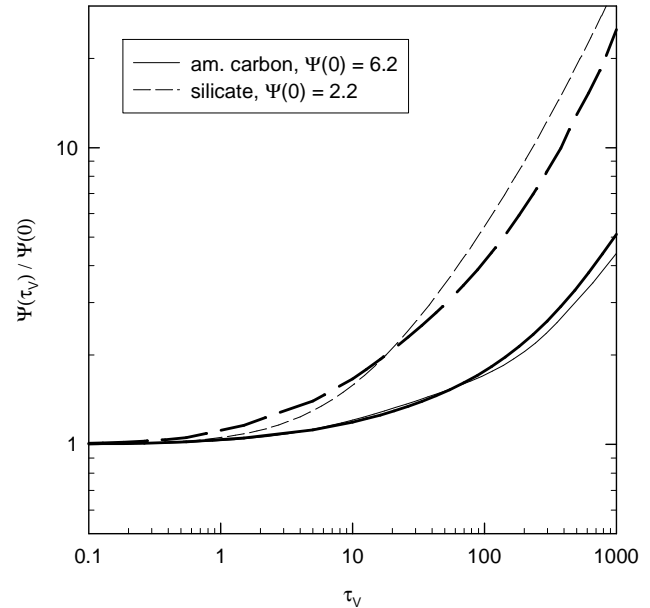


Figure 1. Variation of the scaling function Ψ (equation 15) with overall visual optical depth τ_V in the “standard model” (see text). Thick lines are the results of exact numerical calculations, the thin lines are the analytical approximations of equation B7.

τ_V at large optical depths.[†] Indeed, the numerical results are well described by the simple analytical fit

$$\frac{\Psi(\tau_V)}{\Psi(0)} \simeq 1 + 0.005 \tau_V^m, \quad (33)$$

where the power m is 1 for amorphous carbon and 1.25 for silicate grains. This provides an adequate approximation for Ψ of the “standard model” over the entire displayed range, the accuracy is better than 20% for amorphous carbon, 40% for silicates.

Figure 2 shows the spatial temperature profile for various τ_V . With the density profile $\eta = y^{-2}$, the gray-opacity result gives a temperature drop $T \propto y^{-3/4}$ in the inner regions $y \lesssim \tau_V$, followed by a more moderate decline $T \propto y^{-1/2}$ at larger radii. Qualitatively, this is the behavior displayed in the figure, the actual absorption efficiencies only modify the details.

Figure 3 displays the variation of the SED with overall optical depth. The shape of the SED is governed by some general characteristics, common to all solutions. Because the dust cannot be warmer than T_{sub} , dust emission is negligible for $\lambda \lesssim \lambda_p(T_{\text{sub}})$ and scattered light dominates the diffuse component at these wavelengths. As τ_V increases beyond ~ 10 , the external radiation and scattered light are completely absorbed and dust emission dominates at all relevant wavelengths. At each wavelength λ , dust radiation is generated at radius y where $T(y) \sim (40 \mu\text{m}/\lambda) \times 100 \text{ K}$ (equation 31). For optically thick configurations, Kwan & Scoville (1976)

[†] Formally, this shows that $\Psi \rightarrow \infty$ when $\tau_V \rightarrow \infty$ with all other properties held fixed, and the inner radius of the shell increases without bound (equation 27). However, the solutions are derived assuming steady-state and the time to reach this stage diverges too in that limit.

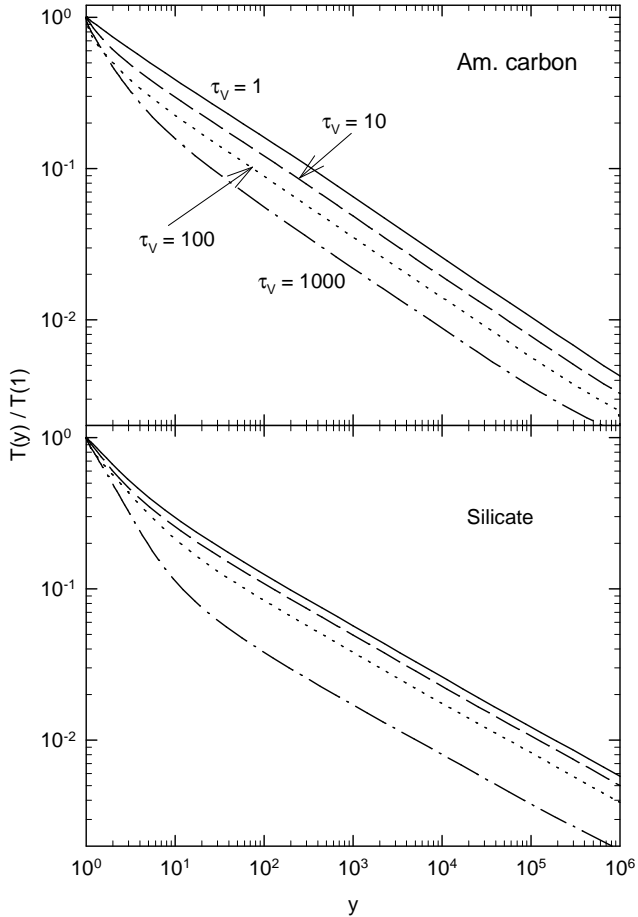


Figure 2. The radial variation of dust temperature in the “standard model” for various optical thicknesses, as indicated.

noted that the SED peaks at the wavelength corresponding to $\tau_\lambda \sim 1$. At longer wavelengths, the source is always optically thin and the spectral shape is independent of overall optical depth. In this region, the shape of the SED reflects only the long-wavelength behavior of the absorption coefficient and the density distribution. The net result of all these effects is that in optically thick shells, the SED roughly retains its shape, shifting as a whole to longer wavelengths as τ_V increases.

This qualitative discussion adequately explains the general behavior of spectral shapes. We proceed now to explore the effects of different input properties on the SED, varying them one by one over the entire plausible range; the properties not varied are those of the “standard” model.

5.1 External spectral shape $f_{e\lambda}$

When the external radiation has a black-body spectral shape with a temperature T_e , $f_{e\lambda} = b_\lambda(T_e)$. Figure 4 displays the effect of varying T_e from 2500 K to 20000 K at various optical thicknesses. In all cases, longward of 10 μm T_e has virtually no effect on the observed spectral shape. The only minor effect of T_e , with no practical observational implications, is to slightly modify the relative scale of emission. The weak dependence on T_e was also a result of RR. The reason $f_{e\lambda}$ has no effect at long wavelengths is that the external

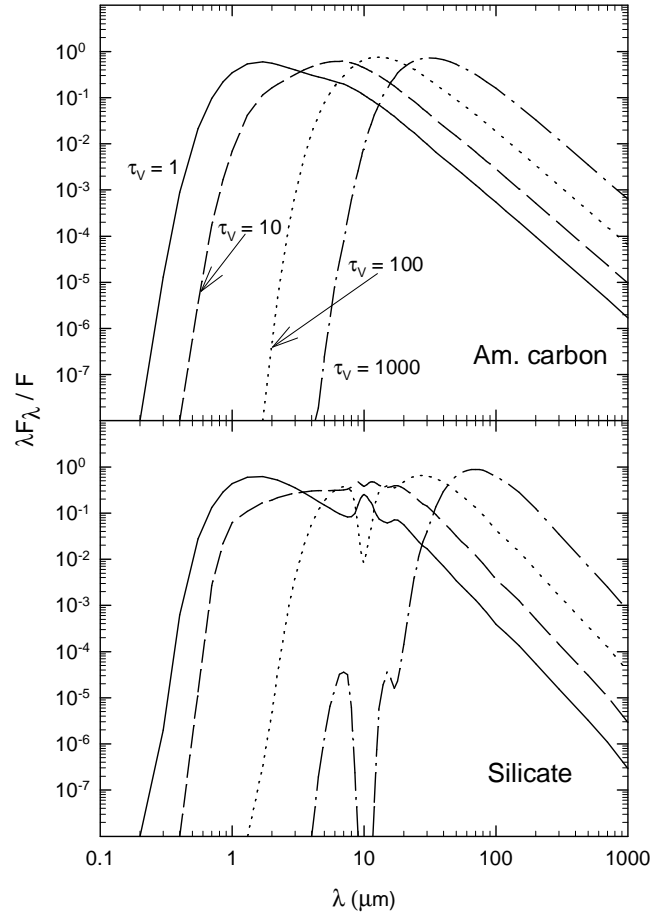


Figure 3. The spectral energy distribution of the “standard model” for various optical thicknesses, as indicated.

contribution is negligible there in comparison with the dust emission; although the source is brighter, the dust emission covers a much larger surface area. The external radiation emerges at short wavelengths because dust emission disappears at $\lambda \lesssim \lambda_p(T_{\text{sub}})$. However, even in that spectral region the external radiation is visible only when $\tau_V \lesssim 1$. At larger optical depths it is fully absorbed, becoming irrelevant at all wavelengths. Therefore, the external spectral shape can be determined only in short-wavelength observations when the optical thickness is not too large. This conclusion applies to all external spectral shapes, not just those that follow Planck’s law.

5.2 Dust sublimation temperature T_{sub}

Figure 5 displays the effect of T_{sub} on the observed spectral shape. As expected, T_{sub} variations have no effect on the shape of the SED at wavelengths shorter than $\lambda_p(T_{\text{sub}})$. At longer wavelengths, varying T_{sub} affects only the scale of the SED not its shape, similar to the effect caused at those wavelengths by variations of T_e . Furthermore, at large optical depths ($\tau_V \gtrsim 100$), spectra produced by varying T_{sub} are indistinguishable at all wavelengths from those produced by varying τ_V . As a result, uncertainty in T_{sub} translates into an uncertainty in the optical depth obtained from a fit to the observed SED.

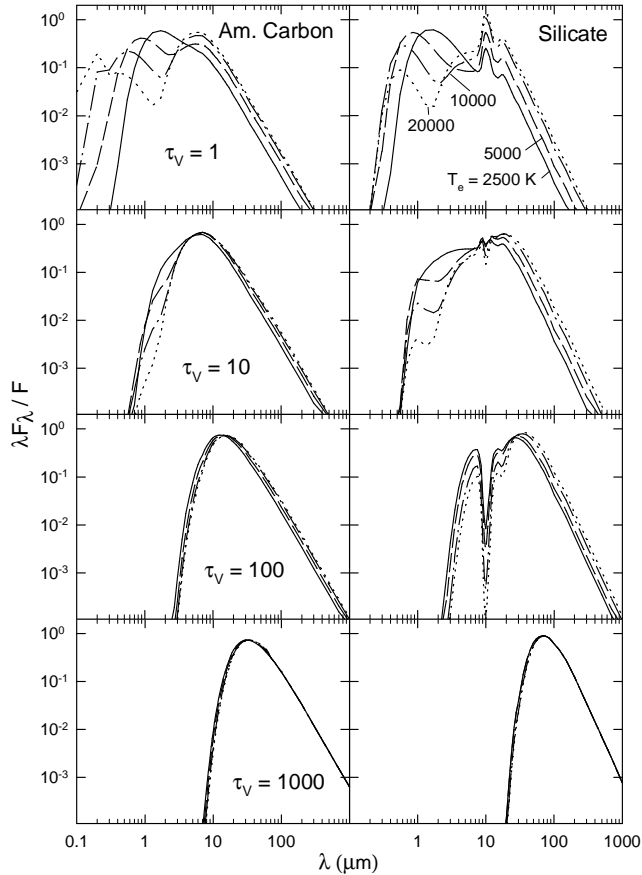


Figure 4. Effect of the external radiation spectral shape on the emerging SED for various optical thicknesses, as marked. The external spectral shape is that of a black-body with temperature T_e as indicated in the top right panel. In this and all subsequent figures, the fixed properties are those of the “standard model”.

Because the impact of T_{sub} on the spectral shape is minor and poorly separated from other effects, T_{sub} cannot be well determined from the SED. The only regime where such determination can be realistically attempted is intermediate optical depths, $\tau_V \sim 10$. In general, the dust sublimation temperature is more reliably determined in high-resolution observations whenever they are capable of resolving the dust condensation zone. From equation 14,

$$\sigma T_1^4 = \Psi \frac{F_{\text{obs}}}{\theta_{1,\text{obs}}^2} \quad (34)$$

where F_{obs} and $\theta_{1,\text{obs}}$ are, respectively, the observed flux and dust condensation zone angular diameter (see also IE96). Whenever feasible, this is the more practical method and we have successfully employed it for analysis of IRC+10216 (Ivezić & Elitzur, 1996b).

5.3 Dust distribution η

Figures 6 – 8 display the effect of the dust density distribution, presenting the results for power-law variation $\eta \propto y^{-p}$ for various non-negative p . As is evident from these figures, for given dust optical properties η is the input quantity with the most substantial impact on the long wavelength emission, the only one to produce an unambiguous observational

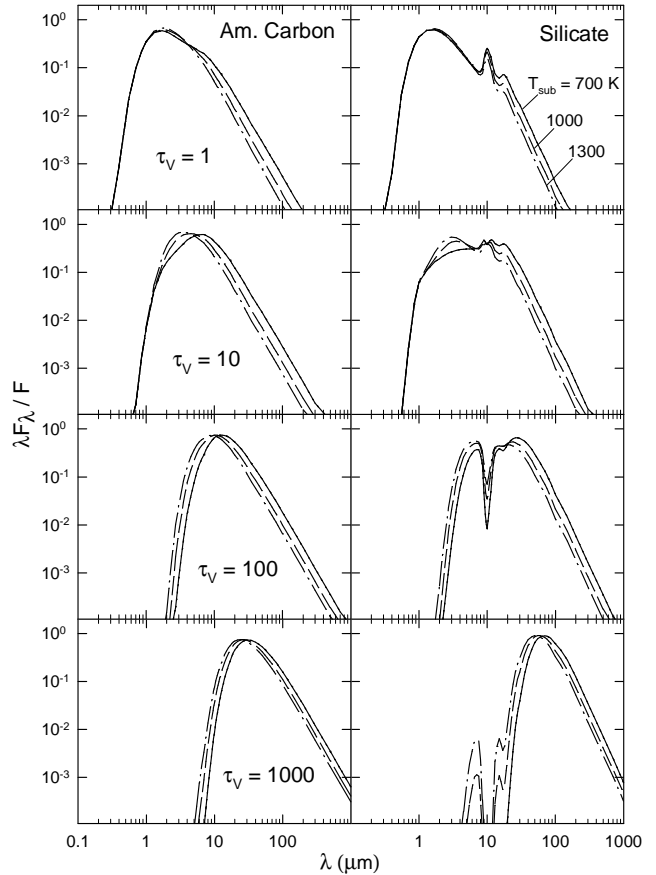


Figure 5. Effect of dust sublimation temperature T_{sub} , indicated in the top right panel, on the emerging SED.

signature. Different density distributions can be easily distinguished by colors involving $\lambda \gtrsim 10 \mu\text{m}$.

Varying the dust density distribution affects the emerging spectrum in two ways. It changes the amount of dust responsible for the emission at a given wavelength and it also modifies the temperature profile. However, the differences between the temperature profiles play only a secondary role to those in the matter distribution itself. The flux at wavelength λ is dominated by emission from radius y where the dust temperature T obeys $\lambda_p(T) \sim \lambda$, so redistributing the material between the various radii directly modifies the spectral shape. Power-law distributions with $p \leq 1$ must include a cutoff to ensure finite column density. We therefore make a distinction between two families of distributions, discussed separately.

5.3.1 Steep distributions; $p > 1$

Steep density distributions do not require a cutoff. Figure 6 displays the SEDs for $p = 2, 3/2$ and $1 + \epsilon$, where $\epsilon \ll 1$. The spectral shapes become flatter at long wavelengths as p decreases since for the same overall optical depth, relatively more material is placed at larger radii (i.e., low temperatures). In particular, for power-law variations $q_{a\lambda} \propto \lambda^{-\beta}$ and $\eta \propto y^{-p}$, Harvey et al. (1991) show that $\lambda f_\lambda \propto \lambda^{-(\beta+4)(p-1)/2}$ in the optically thin regime. We find this relation useful for qualitative understanding of the SED past its peak. Since the differences among SEDs reflect dust

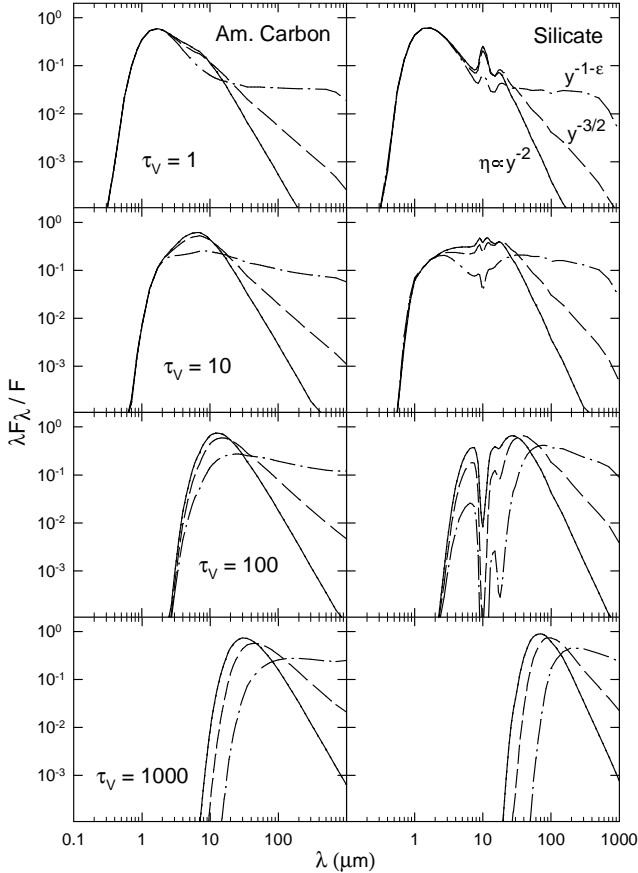


Figure 6. Effect of dust density profile η on the emerging SED for power-law profiles steeper than y^{-1} , indicated in the top right panel.

emission, these differences disappear at $\lambda \lesssim \lambda(T_{\text{sub}})$. Indeed, as the figure shows, the spectral shapes are indistinguishable at such wavelengths, therefore the density distribution cannot be determined from the observed SED at $\lambda \lesssim \lambda(T_{\text{sub}})$. At large optical depth, $\tau_V \gtrsim 50$, the emission peak shifts to wavelengths longer than $\lambda(T_{\text{sub}})$ and the SEDs differ from each other on both sides of the peak.

5.3.2 Flat distributions; $p \leq 1$

Power-law distributions with $p \leq 1$ require a cutoff y_{out} to ensure a finite column density, introducing an additional independent parameter, the shell relative thickness $Y = y_{\text{out}} - 1$. This introduces in turn a lower limit for the temperature and a corresponding wavelength $\lambda_{\text{out}} = \lambda_p(T(y_{\text{out}}))$. Dust emission is mostly confined to wavelengths shorter than λ_{out} , which thus serves as an effective long-wavelength cutoff for the SED.

The cutoff effect is best seen by comparing the SEDs for $\eta \propto y^{-1}$ of figure 7 to those displayed in figure 6 for $\eta \propto y^{-(1+\epsilon)}$. The latter density distribution does not require a y -cutoff and displays the intrinsic effect of this power law for an infinite shell. The strict y^{-1} distribution must include a cutoff, which is varied in figure 7 over a wide range. For all practical purposes, the SED for $Y = 10^5$ is indistinguishable from that for the infinite shell. The difference between the two is noticeable only at wavelengths longer than ~ 300

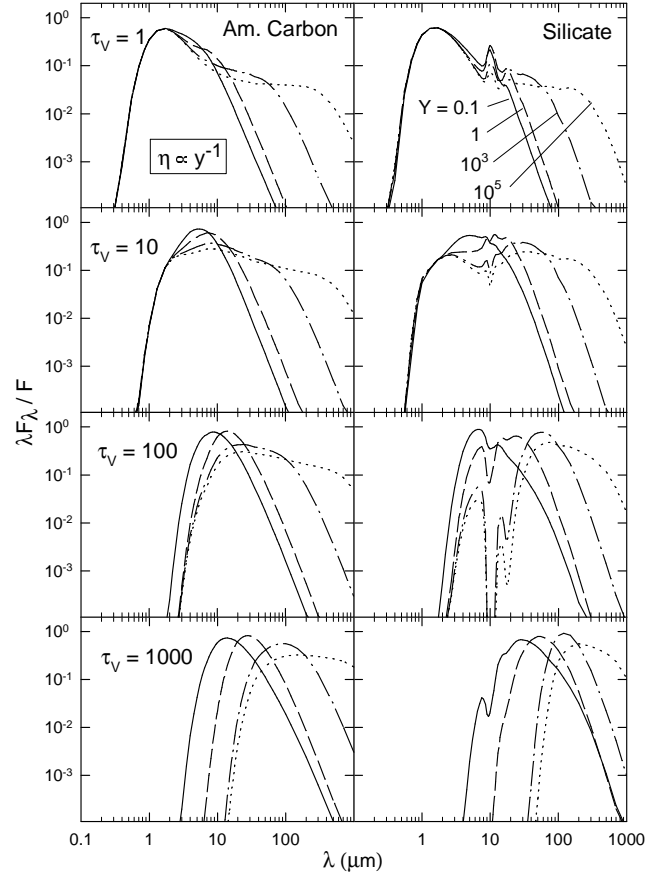


Figure 7. Effect of the shell's geometrical thickness on the emerging SED for dust density profile $\eta \propto y^{-1}$. Only the relative thickness $Y = \Delta r/r_1$, indicated in the top right panel, is relevant

μm , where the SED of the finite shell dips down. As the cutoff Y decreases, λ_{out} decreases too as more cold dust is removed from the shell and the decline of the SED is pushed to shorter wavelengths.

Figure 8 presents the SEDs for constant-density shells with various thicknesses. The gray-opacity result of equation B9 yields

$$\lambda_{\text{out}} \propto [3\tau_V(Y+1) + (Y+1)^2]^{1/4} \quad (35)$$

for such shells when they are not too thin either physically ($Y \gg 1$) or optically ($\tau_V \gg 1$). This simple relation explains adequately the behavior of the long-wavelength cutoff evident in the various panels of figure 8. When $Y \ll \tau_V$, the cutoff wavelength varies in proportion to $(\tau_V Y)^{1/4}$. When $Y \gg \tau_V$, the cutoff wavelength becomes independent of τ_V and varies in proportion to $Y^{1/2}$. In geometrically-thin ($Y \ll 1$) optically-thick ($\tau_V \gg 1$) shells, the cutoff wavelength varies in proportion to $\tau_V^{1/4}$, independent of the shell geometrical thickness.

It is important to note that, although steep density distributions do not require a formal cutoff, in practice such cutoffs always exist because of the finite sizes of dust shells. These finite sizes affect the long wavelength part of the SED in exact analogy to the cutoff of a flat distribution. The finite size of a steep density distribution is relevant only for observations at wavelengths longer than the corresponding λ_{out} . In all cases, the cutoff effect can be easily masked by

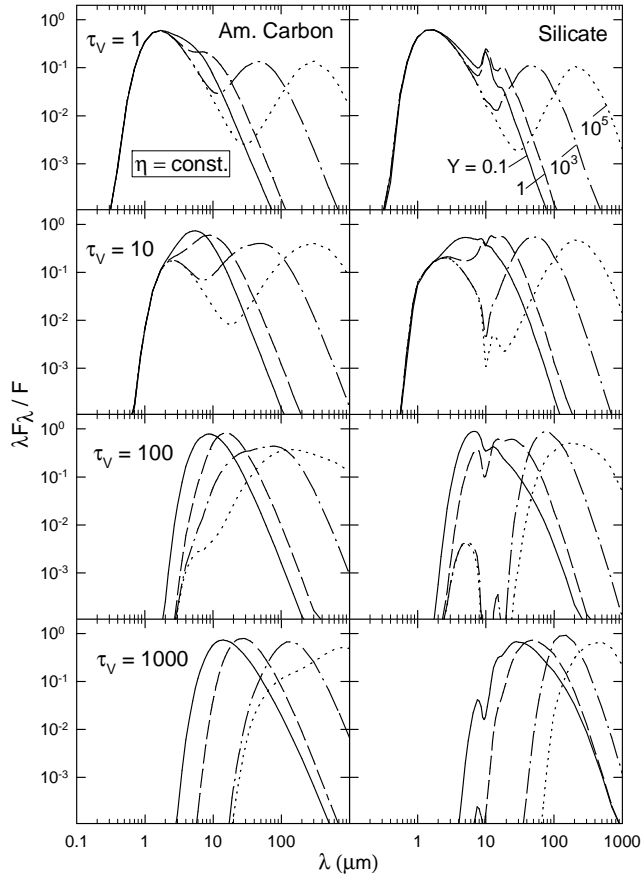


Figure 8. Same as figure 7, but for a constant density distribution.

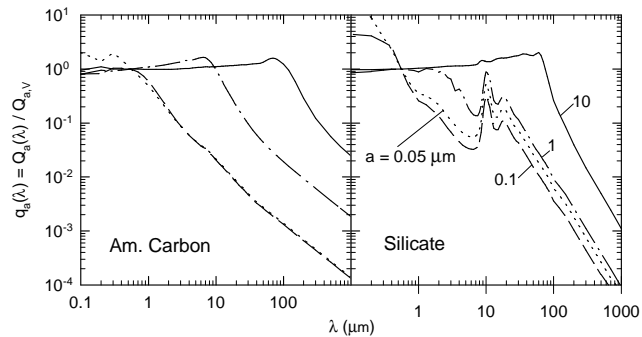


Figure 9. Variation of the absorption efficiency spectral shape with grain radius, indicated in the right panel.

background emission because it generally involves low temperatures.

5.4 Optical properties; grain chemistry and size

The optical properties $q_{a\lambda}$ and ϖ_λ depend on the grain chemical composition and size. The effect of composition on the SED can be discerned in all figures by comparing the panels for amorphous carbon and silicate grains. The significance of grain size a can first be gauged from figure 9. For the two chemical compositions and various radii a it displays $q_{a\lambda}$, obtained from a Mie theory calculation with

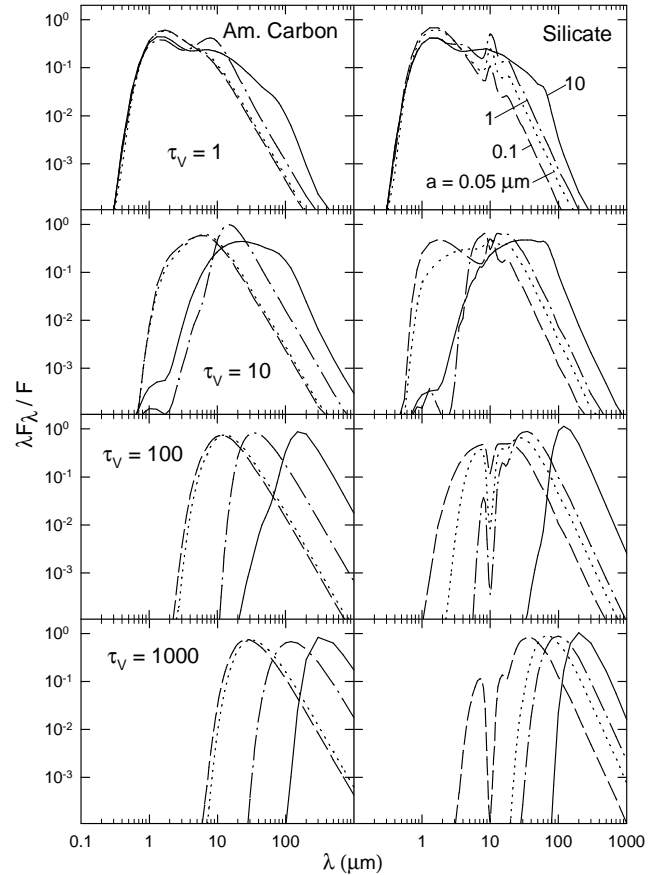


Figure 10. Effect of grain size, indicated in the figure, on the emerging SED.

the appropriate dielectric constants. Except for spectral features, the extinction efficiency is a self-similar function of the scaled variable $2\pi a/\lambda$, approximately constant at short wavelengths and switching to a power-law decline with increasing λ at long wavelengths. In this approximation, the shape of $q_{a\lambda}$ is independent of grain size for $a \lesssim \lambda/2\pi$. Therefore, at wavelengths longer than visual, grain sizes are irrelevant as long as $a \lesssim 0.05 \mu\text{m}$. On the other hand, larger grain radii will significantly affect the results because they are effectively equivalent to selecting grains with different radiative properties. Increasing the grain size beyond $0.05 \mu\text{m}$ amounts to increasing $q_{a\lambda}$ at every wavelength longer than visual. Therefore, for the same τ_V , increasing the grain size increases all far-IR optical depths.

Figure 10 displays the SEDs for our “standard model” with grains of different sizes and various optical depths. The results for all grains smaller than $0.05 \mu\text{m}$ should be the same as for $a = 0.05 \mu\text{m}$. As could be expected, the effect of grain size becomes significant only for $a > 0.1 \mu\text{m}$. The difference between the SEDs for $a = 0.05$ and $0.1 \mu\text{m}$ is generally small, especially for amorphous carbon. Larger grains, $a \gtrsim 1 \mu\text{m}$, generate some structure at intermediate optical depths. This structure, evident in the top two panels for amorphous carbon, arises purely from optical depth effects, reflecting the interplay between the stellar component and dust emission and scattering. It can give a false impression of dust spectral features, although they do not exist in the actual absorption efficiency (see figure 9).

6 DISCUSSION

Scaling has far reaching consequences for modeling and analysis of IR emission from radiatively heated dust. Thanks to scaling, the number of independent input properties is significantly reduced. Only two scales need be specified for a complete solution — the overall optical depth τ_V and the dust sublimation temperature T_{sub} . All other input properties involve only dimensionless, normalized profiles. For the external radiation, only the spectral profile $f_{e\lambda}$ is required. For the dust density, only the normalized distribution η (equation 4) is needed. And for the dust optical properties, only the spectral shapes of absorption and scattering efficiencies enter.

Scaling enables a meaningful systematic study of the observational impact of each independent input property on the emerging IR radiation. The results of the systematic coverage of parameter space presented in the previous section outline the range of spectral shapes produced by spherical configurations. They show which properties delineated in observations can and cannot be explained in this symmetry. For example, the IR spectral shape $\lambda F_\lambda \propto \lambda^{-3/4}$ is sometimes used as an indicator of disk geometry (e.g. Hillenbrand et al. 1992). In fact, this spectral behavior is also produced by spherical distributions with $\eta \propto y^{-p}$ with $p \sim 1.5$ if they are optically thin in the wavelength region where $q_\lambda \propto \lambda^{-\beta}$, since β is typically 1–2 (Miroshnichenko, Ivezić & Elitzur 1997).

Our results suggest a natural classification scheme for IR spectra. For given grain optical properties, every η produces a distinct family of solutions, with position within the family determined by τ_V . For the most part, T_{sub} and $f_{e\lambda}$ have only a minor effect. Therefore, the SEDs of all astronomical objects that share the same dust density distribution become a one-parameter family in which each member is fully characterized by its τ_V . This leads to correlations among spectral properties and structure in color-color diagrams. Scaling breaks down when the dust inner boundary is controlled by effects other than dust sublimation. In such sources, the inner-boundary dust temperature T_1 ($< T_{\text{sub}}$) becomes an additional independent parameter, varying with the external flux according to $T_1 \propto F_{e1}^{1/4}$.

Various classes of astronomical objects show evidence for scaling, indicating that in these sources the dust inner boundary is controlled by sublimation. A common spectrum for compact HII regions was noted in Rowan-Robinson (1979) and modelled in RR. This was further emphasized by Wood and Churchwell (1989), who point out that for all ultra-compact HII regions observed by IRAS, “the shapes of flux density distributions are strikingly similar”, a fact also recognized by Chini et al. (1986). The trends observed among spectral properties of IR radiation from young stellar objects elicited a number of classification schemes. Adams, Lada & Shu (1987) employed the slope of the SED, Adams (1990) the visual extinction derived from model spectra, Ladd et al. (1991) the mean frequency of the spectrum and Myers & Ladd (1993) the corresponding bolometric temperature. Myers & Ladd also noted that all these schemes are equivalent, but the reasons for the trends and for this equivalence were not clear. Scaling provides a simple explanation for both. Furthermore, various distributions presented in Myers & Ladd show that IR spectral properties

are indeed independent of luminosity, as prescribed by scaling. Finally, the structure in color-color diagrams implied by scaling had been noticed in the IRAS colors of a variety of objects. These include T Tau stars (Harris, Clegg & Hughes, 1989), BN objects (Henning, Pfau & Altenhoff, 1990), HII regions (Hughes & MacLeod, 1989; Wood & Churchwell, 1989), H₂O masers in star-forming regions (Wouterloot & Walmsley, 1986) and late-type stars (van der Veen & Habing, 1988). Various scaling properties of the latter were noted previously by Rowan-Robinson and Harris (1983 and references therein).

Dusty winds around late-type stars provide an even tighter form of scaling (IE95, IE96). The structure of these winds is controlled by radiation pressure on the dust grains, therefore the density distribution η need not be prescribed in advance. Instead it is determined from the hydrodynamics coupled to the radiative transfer, and the solution does not require any other parameter in addition to optical depth. Therefore, IR emission from all late-type stars with a given dust composition can be fully classified in terms of a single parameter, τ_V . Detailed analysis shows that the data fully corroborate all the correlations predicted by scaling for these sources. We are in the midst of a study that extends this detailed analysis to the IRAS data for all the Galactic point sources. The scaling correlations displayed by these data will enable us to identify the dust density distributions of various classes of Galactic objects. The results of this study will be reported separately in a forthcoming publication.

ACKNOWLEDGMENTS

We thank the referee Dr. M. Rowan-Robinson for his careful reading and useful comments which helped improve the manuscript. Support by NSF grant AST-9321847, NASA grant NAG 5-3010 and the Center for Computational Sciences of the University of Kentucky is gratefully acknowledged.

REFERENCES

- Adams, F.C., Lada, C.J., Shu, F.H., 1987, ApJ, 312, 788
- Adams, F.C., 1990, ApJ, 363, 578
- Auer, L.H., 1984, in *Methods in Radiative Transfer*, ed. W. Kalkofen (Cambridge: Cambridge University Press), p. 237
- Chini, R., et al., 1986, A&A, 154, L8
- Hanner M.S., 1988, *Infrared Observations of Comets Halley and Wilson and Properties of the Grains (NASA89-13330)*, 22
- Harris, S., Clegg, P., Hughes, J., 1989, MNRAS, 235, 441
- Harvey, P.M., Lester, D.F., Brock, D., Joy, M., 1991, ApJ, 368, 558
- Henning, Th., Pfau, W., Altenhoff, W.J., 1990, A&A, 227, 542
- Hillenbrand, L.A., Strom, S.E., Vrba, F.J., & Keene, J. 1992, ApJ 397, 613
- Hughes, V.A., MacLeod, G.C., 1989, AJ, 97, 786
- Ivezić, Ž., Elitzur, M., 1995, ApJ, 445, 415 (IE95)
- Ivezić, Ž., Elitzur, M., 1996a, MNRAS, 279, 1011 (IE96)
- Ivezić, Ž., Elitzur, M., 1996b, MNRAS, 279, 1019
- Ivezić, Ž., Groenewegen, M., Men'shchikov, A., Szczerba, R., 1997, in preparation
- Ivezić, Ž., Nenkova, M., Elitzur, M., 1997, User Manual for DUSTY, Internal Report, University of Kentucky, accessible at <http://www.pa.uky.edu/~moshe/dusty>

- Kwan, J., Scoville, N., 1976, ApJ, 209, 102
 Ladd, E. F., et al., 1991, ApJ, 366, 203
 Laor, A., Draine, B.T., 1993, ApJ, 402, 441
 Leung, C.M., 1976, ApJ, 209, 75
 Mihalas, D., 1978, Stellar Atmospheres (San Francisco: W. H. Freeman), chapter 2
 Milne, E.A., 1921, MNRAS, 81, 382
 Miroshnichenko, A., Ivezić, Ž., Elitzur, M. 1997, ApJ 475, L00
 Myers, P.C., Ladd, E.F., 1993, ApJ, 413, L47
 Ossenkopf, V., Henning, Th., Mathis, J.S., 1992, A&A, 261, 567
 Rowan-Robinson, M., 1979, ApJ, 234, 111
 Rowan-Robinson, M., 1980, ApJS, 44, 403 (RR)
 Rowan-Robinson, M., 1982, in Submillimetre Astronomy, ed. P. Phillips and J. Beckman (Cambridge: Cambridge University Press), p. 47
 Rowan-Robinson, M., Harris, S., 1983, MNRAS, 202, 797
 Schmid-Burgk, J., 1975, A&A, 40, 249
 van der Veen, W.E.C.J., Habing, H.J., 1988, A&A, 194, 125
 Wood, D.O.S., Churchwell, E., 1989, ApJ, 340, 265
 Wouterloot, J.G.A., Walmsley, C.M., 1986, A&A, 168, 237

APPENDIX A: GRAIN MIXTURES

When the dust is composed of different types of grains, its extinction coefficient is

$$\kappa_\lambda = \rho_d \sum_i p_i \frac{\pi a_i^2}{m_i} Q_{\lambda i}. \quad (\text{A1})$$

Here ρ_d is the overall dust density and p_i is the fraction of that density due to the i -th component ($\sum p_i = 1$). The mass, radius and extinction efficiency of a single grain from this component are denoted m_i , a_i and $Q_{\lambda i}$, respectively. The different components reflect possible variations of chemical composition and/or grain size. For simplicity we treat the components as discrete; generalization to the continuous case is trivial. With the aid of equation 6, the dust source function is

$$S_\lambda = \sum_i x_{\lambda i} \left[(1 - \varpi_{\lambda i}) B_\lambda(T_{d,i}) + \varpi_{\lambda i} \int I_\lambda(\Omega') g_i(\Omega', \Omega) \frac{d\Omega'}{4\pi} \right], \quad (\text{A2})$$

where $\varpi_{\lambda i}$ and g_i are, respectively, the albedo and angular phase function of the i -th component and

$$x_{\lambda i} = \frac{p_i (\pi a_i^2 / m_i) Q_{\lambda i}}{\sum_i p_i (\pi a_i^2 / m_i) Q_{\lambda i}} \quad (\text{A3})$$

is the weight of its contribution to the extinction coefficient at wavelength λ . Each component may have a different temperature, $T_{d,i}$, determined from overall flux conservation. This equilibrium relation becomes a vanishing sum of the fractions p_i with coefficients that depend on the corresponding individual temperatures $T_{d,i}$. Since the temperature of a dust component cannot depend on its relative abundance, each coefficient in the sum must vanish separately. This produces the temperature equation of the i -th component

$$\int q_{a\lambda,i} B_\lambda(T_{d,i}) d\lambda = \int q_{a\lambda,i} J_\lambda d\lambda, \quad (\text{A4})$$

where $q_{a\lambda,i} = q_{\lambda i} (1 - \varpi_{\lambda i}) / (1 - \varpi_{\lambda 0i})$ is the absorption efficiency of the i -th component normalized to the fiducial wavelength λ_0 , analogous to equation 9 for a single-component dust.

A convenient indexing of the dust components is by decreasing sublimation temperature. Consider a spherically symmetric configuration with a prescribed radial variation of overall dust density when the shell inner radius is controlled by sublimation of the first component at temperature $T_{\text{sub},1}$. The problem is identical to that of a single-component dust as long as the temperature of component 2 at dimensionless radius y , determined from equation A4, remains higher than its sublimation temperature $T_{\text{sub},2}$. The radius y_2 at which component 2 is included in the mix is thus determined from radiative transfer, and so on. The only difference in the solution procedure from the case of single-type dust is that the dimensionless density profile $\eta(y)$ cannot be fully prescribed beforehand since the determination of the sublimation radii y_2, y_3 , etc., requires solution of the radiative transfer problem. Scaling is preserved but the exact form of $\eta(y)$ requires an iterative procedure. The extension of this procedure to arbitrary geometries is straightforward.

APPENDIX B: APPROXIMATE SOLUTIONS IN SPHERICAL SYMMETRY

The radial variation of temperature requires the spatial profile of J_λ , equivalent to the spatial variation of both the overall radiative energy density $J(y) = \int J_\lambda(y) d\lambda$ and the frequency profile J_λ/J . The former can be obtained from the wavelength-integrated radiative moment equations when they are closed by some suitable approximation. Auer (1984) proposed the closure relation

$$3P = 4\pi J + 2F, \quad (\text{B1})$$

where P is the bolometric radiation pressure, obtained from the second angular moment of the intensity. This relation improves on the classic Eddington approximation ($3P = 4\pi J$) by providing the correct behavior in both the optically thin and thick limits. With this approximation, the radiation-pressure equation becomes

$$4\pi \frac{dJ}{dy} = -\frac{F_1}{y^2} \left[\frac{2}{y} + 3\tau_0 q_F(y) \eta(y) \right], \quad (\text{B2})$$

where

$$q_F = \int q_\lambda f_\lambda d\lambda \quad (\text{B3})$$

is the extinction efficiency averaged with the flux spectral shape. Solution of this equation requires a boundary condition. We assume that the energy density vanishes when $y \rightarrow \infty$, setting aside for a moment the case of finite shells. Then the solution is

$$4\pi J(y) = F_1 \left[\frac{1}{y^2} + 3\tau_0 \int_y^\infty q_F(y) \eta(y) \frac{dy}{y^2} \right]. \quad (\text{B4})$$

This result requires the flux-averaged q_F , which cannot be calculated without the spectral shape of the diffuse component of the flux (see equation 29). We will approximate this with the Planck spectral shape at the local temperature, namely $F_{d\lambda} \propto b_\lambda(T)$. This can be expected to give an adequate approximation at large optical depths, less so at small ones, where the significance of the diffuse component is diminished anyhow. With this approximation,

$$q_F(y) = \int q_\lambda f_{e\lambda} e^{-\tau_\lambda(y)} d\lambda$$

$$+ q_{\text{P}}(T(y)) \left(1 - \int f_{\text{e}\lambda} e^{-\tau_{\lambda}(y)} d\lambda \right). \quad (\text{B5})$$

This completes the approximation for J . Next we need the spectral shape of the diffuse component $J_{\text{d}\lambda}$. This can be reasonably expected to resemble the spectral shape of the diffuse flux $F_{\text{d}\lambda}$, so we approximate it, too, with $b_{\lambda}(T)$. Then the radiative equilibrium equation (9) gives

$$4\pi J(y) = 4\sigma T^4 + \frac{F_1}{y^2} \int f_{\text{e}\lambda} e^{-\tau_{\lambda}(y)} \left(1 - \frac{q_{\text{a}\lambda}}{q_{\text{aP}}(T)} \right) d\lambda. \quad (\text{B6})$$

Equations B4 and B6 produce the temperature profile as a function of y , with F_1 , or equivalently Ψ (see equation 14), obtained from the expressions at $y = 1$. The results are

$$\begin{aligned} \Psi \times \left(\frac{T}{T_1} \right)^4 &= \frac{1}{y^2} \left[1 - \int f_{\text{e}\lambda} e^{-\tau_{\lambda}(y)} \left(1 - \frac{q_{\text{a}\lambda}}{q_{\text{aP}}(T)} \right) d\lambda \right] \\ &\quad + 3\tau_0 \int_y^\infty q_{\text{F}}(y) \eta(y) \frac{dy}{y^2}, \\ \Psi &= \frac{q_{\text{ae}}}{q_{\text{aP}}(T_1)} + 3\tau_0 \int_1^\infty q_{\text{F}}(y) \eta(y) \frac{dy}{y^2}; \end{aligned} \quad (\text{B7})$$

note that equation 30 is recovered when $\tau_0 = 0$. Together with equation B5, this completes the solution for the temperature profile for any given density profile η that extends to infinity. The solution is only in implicit form because T enters on the right-hand-side through the Planck-averages $q_{\text{P}}(T)$ and $q_{\text{aP}}(T)$. Therefore the complete solution requires iterations, but these are straightforward and converge rapidly. We find that these analytic results provide an excellent approximation for the exact solutions, typically within 10%.

When the shell is finite, a boundary condition must be specified for its energy density at the outer edge y_{out} . From the definitions of J and F as angular moments of the intensity it follows that

$$4\pi J(y_{\text{out}}) = \frac{\gamma F_1}{y_{\text{out}}^2}, \quad (\text{B8})$$

where γ varies from 1 when the angular distribution of the emergent radiation is directional to 2 when it is isotropic. Leaving γ as an unknown factor, this term is just added to the solution on the right-hand-side of equation B4, simply adding γ/y_{out}^2 to the right-hand-side of the two relations in equation B7. So the analytic approximation for finite shells includes a term that remains uncertain to within a factor of 2. However, this term is significant only in shells that are thin both physically and optically ($y_{\text{out}} - 1$, $\tau_0 < 1$) and our numerical results show that $\gamma \simeq 1.5$ is an adequate approximation in virtually all cases.

A different approximate solution scheme was proposed in RR. That scheme does not fully incorporate scattering but its iterations include a variable Eddington factor, therefore it is in principle capable of convergence to the exact solution in the absence of scattering. Since our scheme involves a prescribed Eddington factor (eq. B1) it only converges to an approximate solution, not the exact one. However, when scattering is important it has the edge and we usually obtain a level of accuracy comparable to RR with significantly fewer computations, mostly because we do not have angular integrations. Furthermore, our approximate solution becomes fully explicit in the ‘‘gray opacity’’ case, the approximation that assumes frequency independent extinction. Then $q_{\lambda} =$

1 and the solution reverts to the simple, explicit form

$$\begin{aligned} \Psi \times \left(\frac{T}{T_1} \right)^4 &= \frac{1}{y^2} + 3\tau_0 \int_y^\infty \eta(y) \frac{dy}{y^2}, \\ \Psi &= 1 + 3\tau_0 \int_1^\infty \eta(y) \frac{dy}{y^2}. \end{aligned} \quad (\text{B9})$$

In the case of a finite shell, the right-hand-sides of both equations again are augmented by γ/y_{out}^2 . This gray-opacity result follows directly from the Auer closure relation and does not require assumptions about the spectral shape of the diffuse component. It provides a closed-form expression that readily explains many properties of the full solutions, as pointed out in section 5.

APPENDIX C: NUMERICAL PROCEDURES

The code DUSTY, which solves the spherical radiative transfer problem employing the scaling approach described here, is publicly available for general use (Ivezic, Nenkova & Elitzur 1997). The numerical calculations are conveniently performed with the aid of the dimensionless energy density

$$u_{\lambda} = \frac{4\pi y^2}{F_{\text{e}1}} J_{\lambda}. \quad (\text{C1})$$

Extracting the y^2 radial dilution reduces the dynamic range of the density, helping the numerical accuracy. For isotropic scattering, u_{λ} at radius y obeys the integral equation

$$\begin{aligned} u_{\lambda}(y) &= f_{\text{e}\lambda} e^{-\tau_{\lambda}(y)} \\ &\quad + \frac{1}{2} \int \left[\varpi_{\lambda} u_{\lambda}(y') + (1 - \varpi_{\lambda}) \Psi \left(\frac{T'}{T_1} \right)^4 b_{\lambda}(T') \right] \\ &\quad \times e^{\tau_{\lambda}(y', \mu) - \tau_{\lambda}(y, \mu)} \left(\frac{y}{y'} \right)^2 d\tau_{\lambda}(y', \mu) d\mu, \end{aligned} \quad (\text{C2})$$

where $\mu = \cos \theta$. In this equation $T' = T(y')$ is obtained from

$$\frac{q_{\text{aP}}(T')}{q_{\text{aP}}(T_1)} \left(\frac{T'}{T_1} \right)^4 = \frac{\int q_{\text{a}\lambda} u_{\lambda}(y') d\lambda}{\int q_{\text{a}\lambda} u_{\lambda}(1) d\lambda} \quad (\text{C3})$$

and Ψ from

$$\Psi = \frac{1}{q_{\text{aP}}(T_1)} \int q_{\text{a}\lambda} u_{\lambda}(1) d\lambda. \quad (\text{C4})$$

Once a radial grid is prescribed, the numerical evaluation of the integral of any radial function is transformed into multiplication with a matrix of weight factors determined purely by the geometry (cf Schmid-Burgk, 1975). Therefore, if $T(y)$ and Ψ are given, u_{λ} can be obtained for all radial grid points through matrix inversion. This provides a direct solution to the full scattering problem, obviating the need to iterate over $u_{\lambda}(y)$ itself.

We start the calculation with $T(y)$ and Ψ from the analytic solution of appendix B, calculate the corresponding $u_{\lambda}(y)$ and iterate until convergence. Because the scattering problem is solved directly by the matrix inversion, convergence is very rapid; an accuracy of 10^{-4} is achieved with fewer than 10 iterations even for the largest optical depths considered here. The solution is accomplished once the density u_{λ} does not vary, within a prescribed tolerance, when the grid density is increased. The number of radial grid points we needed varied from ~ 20 for moderate optical

depths ($\tau_V \lesssim 10$) to 80 for $\tau_V = 1000$. The number of angular grid points used in the μ -integration is typically 2–3 times the number of radial grid points. Once the energy density u_λ is found, the flux spectral shape $f_\lambda(y)$ is calculated from the same integral with $d\mu$ replaced by $\mu d\mu$.

We have compared our code with a number of benchmark solutions and verified its accuracy to better than 0.1% (Ivezić et al. 1997). Most of the computer time is spent on calculation of the weight matrix for spatial integrations. This matrix is determined purely by geometry and does not vary between iterations, giving our method an edge in calculation speed over other schemes (e.g. iterations over variable Eddington factor). In particular, large optical depths do not increase the computational difficulties as much as they do in purely iterative schemes; we encountered no difficulties with τ_V as large as 2000. In addition, the inclusion of scattering in the direct matrix inversion eliminates the problems that large albedos present in other schemes. Our method remains stable even for albedos that approach unity at some wavelengths.